Article ID: 1006-8775(2010) 02-0143-11

DIAGNOSTIC ANALYSIS OF ASYMMETRIC SPIRAL RAINBANDS AROUND THE LANDING OF TYPHOON HAITANG (2005)

WANG Yong (王 勇)[1], DING Zhi-ying (丁治英)[1], LI Xun (李 勋)[2], WANG Qun (王 群)[3]

(1. School of Atmospheric Science / Jiangsu Key Laboratory of Meteorological Disaster, Nanjing University of Information Science and Technology, Nanjing 210044 China; 2. Meteorological Observatory of Hainan, Haikou 570203 China; 3. Yancheng Meteorological Observatory, Yancheng 224005 China)

Abstract: By using WRF mesoscale model, this paper carries out a numerical simulation and diagnostic analysis of the structural characteristics of the asymmetric spiral rain bands around the landing of Typhoon Haitang during the period of July 19 to 20, 2005. The result indicated that the two rainbands associated with the precipitation centre was mainly located northeast of the typhoon centre. The movement and intensity of the southern rainband corresponded well with the 850-hPa positive vorticity band from 0200 to 1800 UTC July 19, 2005. Under the effect of cyclonic circulation, the positive vorticity band at 850 hPa connected with a southern rain band, leading to the intensification of rainfall in the southern centre of the precipitation. The southward rainband gradually moved toward and then merges with the northward one, strengthening the rainfall in the northern centre of the precipitation. Besides, the relationship between the heavy rainfall and the divergence field of vertical shear wind in the high altitude is analyzed. Finally, the relationship is revealed between the development of the vertical component of convective vorticity vector and the rainfall near the two centres of precipitation in the low altitude.

Key words: diagnostic analysis; asymmetrical spiral rain bands; vertical shear wind; convective vorticity vector

CLC number: P444 **Document code:** A **doi:** 10.3969/j.issn.1006-8775.2010.02.006

1 INTRODUCTION

In recent years, the calamitous weather brought about by typhoons has resulted in severe damage to the eastern part of China. Therefore, relevant works in this field has been attached more and more importance to. The study of the rainstorm, one of the terrible results of typhoons, especially the asymmetric precipitation, has become a hotly discussed issue. In a study of the fluctuating precipitation of typhoon Matsa in 2005, Li, et al.[1] pointed out that the fluctuating distribution features of the rainbands were related to relevant atmospheric stratification and the features of the mixed waves were made up of proper gravity internal waves and atmosphere inertia waves. In a numerical simulation of the spiral rain bands of Kammuri, an intense tropical storm in 2002, Zhu et al.[2] indicated that the moving speed of the simulated spiral rainbands along the azimuth angle was in line with the theoretical wave celerity of vortex Rossby waves (VRW), accompanied by the radial dispersion of the energy. Zhu et al.[3] discussed the circumfluence, structural features and evolvement of dynamic and heat power of typhoon Winnie (1997) in its stage of transformation. They found that after the landing of the typhoon, the change of the underlying surface caused much asymmetricity to the transportation of the warm and wet vapor from offshore waters, which in turn led to the asymmetric distribution of the thermal structure. The spiral rainband of the typhoon is a primary reflection of its asymmetric structure. With regard to its causes, some researchers[4-6] argued that because of the horizontally uneven distribution of the basic air current, the radial gradient effect of vertical vorticity would generate VRW, the superposition and transmission of which is one of the causes of the spiral rainbands. Besides, due to the complicated structure inside the typhoon, its meso-scale fluctuation is with mixed features of both gravity inertial waves and VRW.

Received date: 2009-11-23; **revised date:** 2010-03-11
Foundation item: National Program on Basic Research Project (973 Program) (2009CB421503); National Natural Science Foundation of China (40775033); National Natural Science Foundation of China (40975037)
Biography: WANG Yong, M.S., mainly undertaking the research on meso-scale weather dynamics.
E-mail for corresponding author: wy92380@163.com

In our meso-scale diagnostic analyses of the rainstorm, some new physical quantities, such as the generalized moist potential vorticity based on the non-uniform saturation of real atmosphere and meso-scale convection vorticity vectors[7-8], were put into more use in the study of the rainstorm.

When Haitang (0505) landed in Fujian province for the second time, the spiral cloud bands in the periphery of the typhoon led to intensive precipitation in Fujian and Zhejiang provinces, which are located in southeast China. The cloud cluster in the southeast supercritical flow also contributed to the intensive precipitation. At present, there are still not many studies on the asymmetrically structured spiral rainbands in the periphery of typhoons. Therefore, this paper centres on the relationship between the movement of the spiral rain bands caused by the landing of Haitang, the asymmetric structure features and the precipitation centre.

2 DATA AND NUMERICAL SIMULATION

Based on NCEP/NCAR grid data with a resolution of 1°×1° and the mesoscale model WRFV2, this paper carries out a numerical simulation and a diagnostic analysis of the rainstorm caused by Haitang in the southern and central areas of Zhejiang province, which occurred from 1900 to 2000 July 19. The schemes for physical processes and numerical simulation are as follows[9]. For dual nesting grid system, the coarse grids are 181×161 and the grid length is 18 km; the fine grids are 169×196 and the grid length is 6 km. The vertical delamination is 28 and the top level is 50 hPa. The parameter schemes for the cumulus convection are so designed that the coarse grids follow the Kain/Fritsch scheme and fine grids follows the Grell scheme, which all take 0000 July 19 as the start of the simulation and the integration lasts for 36 hours.

The verification of the result of this numerical simulation is presented below. From comparisons between the real precipitation from 0000 July 19 to 0000 July 20 and the one simulated by the fine grids, we found that the locations of the two simulated precipitation centres (121°E, 28.2°N and 120°E, 27.2°N) were relatively close to those of the real ones[9]. The simulated precipitation located at 120°E, 27.2°N mainly took place between 0200 and 0900 July 19 and the one located at 121°E, 28.2°N mainly happened between 0900 and 1600 July 19. In real situation, the precipitation located at 120°E, 27.2°N mainly took place between 0000 and 0600 July 19 and the one located at 120°E, 27.2°N mainly happened between 0600 and 1800 July 19. The main period of time and the amount of the simulated precipitation are relatively close to those of the real situation[9] (Fig. 1).

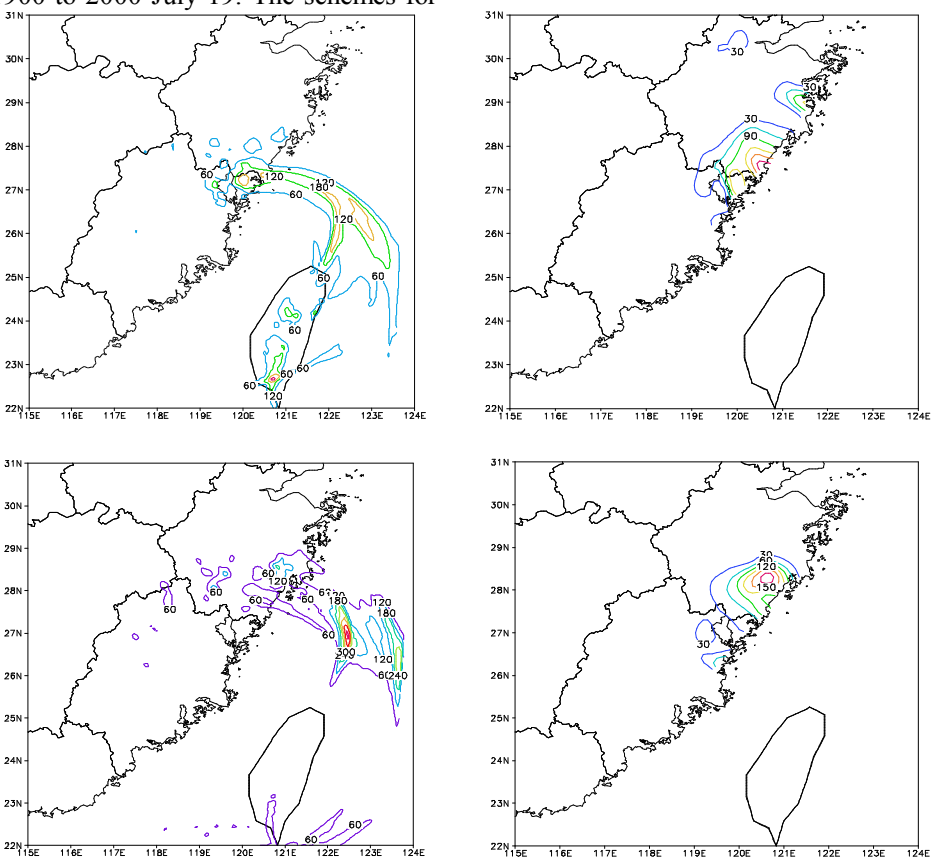

Fig.1 The precipitation simulated by the fine grids (left panels, unit: mm) at 0200 to 0900 and 0900 to 1600 July 19. The real precipitation (right panels, unit: mm) at 0200 to 0900 and 0900 to 1600 July 19.

In order to better verify the systematic transformation features of the typhoon rainbands, this thesis makes use of the TBB data obtained from Project 9201 of National Satellite Centre to observe the changes of the typhoon and its cloud bands. From Fig. 2a it could be seen that at 0600 July 19, asymmetrically structured cloud bands with the principal part over the sea were already linked up with the precipitation bands (Fig. 2b) located at the precipitation centre (120°E, 27.2°N). From Fig. 2c it could be seen that several cloud bands on the continent were combined, corresponding to the fact that the precipitation bands (120°E, 27.2°N) were combined with the rain bands (121°E, 28.2°N) in Fig. 2d. Through analysis of systemic changes and the precipitation amount measured per hour, conclusions can be reached that the transformation features of the spiral cloud bands have been successfully simulated. The precipitation centre located at 120°E, 27.2°N is called the southern centre, and that located at 121°E, 28.2°N the northern centre, of precipitation.

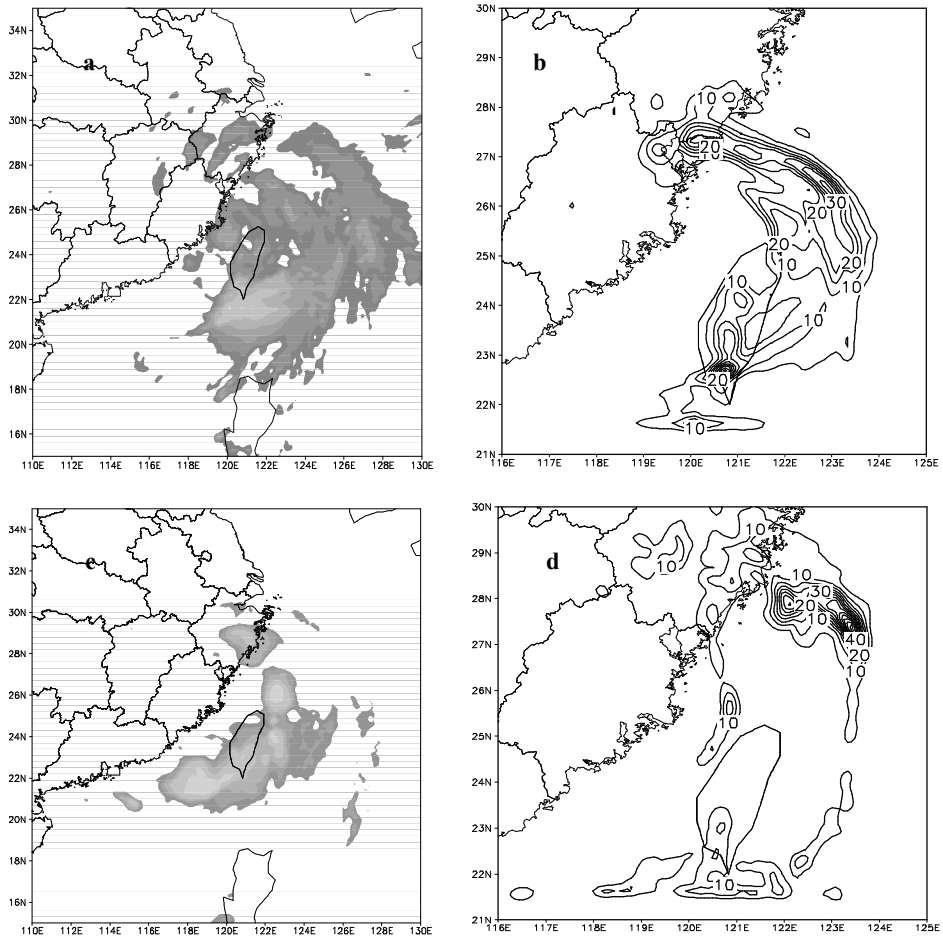

Fig.2 The distribution of TBB cloud bands at 0600 (a) and 1800 (c) July 19; The precipitation simulated by the coarse grids at 0600 to 0700 (b) and 1800 to 1900 (d) July 19. (unit: mm)

Figure 3 shows the route of the typhoon for the 24 hours around its landing, and Fig. 4 shows the air pressure of the typhoon centre. The starting point is 0000 July 19. From the comparison between the effect of the simulated precipitation and route of typhoon and its central air pressure, it could be seen that though the effect of the simulated intensity of typhoon in the early stage is not ideal, the effect of the simulated route and precipitation is in perfect accordance with the real situation. In all, this simulation of the typhoon rainstorm is basically successful, and could be further diagnosed and studied. Except for what is specially pointed out, the rest of the paper will use the simulated data of the fine grids for analysis.

3 STRUCTURAL ANALYSIS OF THE ASYMMETRIC SPIRAL RAIN BANDS

3.1 *Relationship between the precipitation and the radial vertical cross section characteristics of relevant physical quantities of the asymmetrical rain bands*

The spiral rain band is one of the basic characteristics of the typhoon; in the meanwhile, it is

closely connected with typhoon rainstorms. Around the landing of Haitang, there existed many spiral rain bands to the north-east of the centre of the typhoon. The research [2] shows that there is good correspondence between the spiral rain bands in the typhoon and the strong positive vorticity band in low altitudes (Fig. 5). The following is a discussion on the relationship between the asymmetric rain bands and the precipitation. The radial vertical section of relevant physical quantities are graphically sketched by connecting the geometrical centre of the typhoon and the 850-hPa positive vorticity band (the black line in Fig. 5a), and then the figure showing the precipitation amount of each point in the radial direction measured by hour are also drawn. Finally, an analysis of the relationship between the two is carried out.

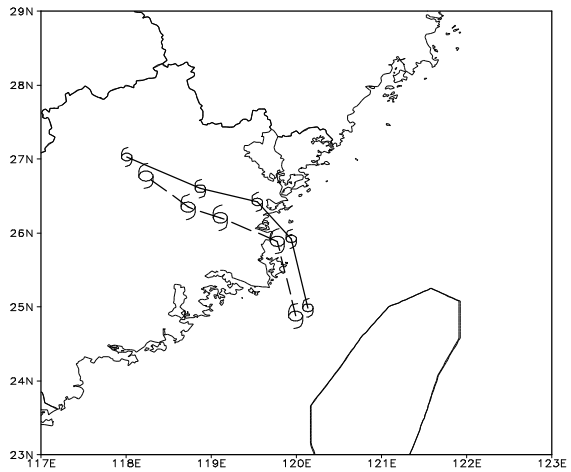

Fig.3 The route of the typhoon for every 6 hours from 0000 July 19 to 0000 July 20.

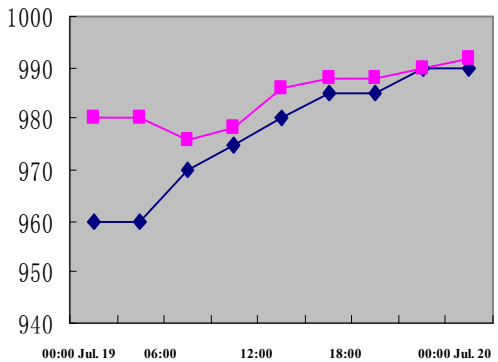

Fig.4 Air pressure at the centre of the typhoon every 3 hours from 0000 July 19 to 0000 July 20. The broken line: the route simulated by the coarse grids; the solid line: the realistic route. Unit: hPa.

About 300 km away to the northeast of the centre of the typhoon, the precipitation of the outer spiral rain bands was relatively heavy (Fig. 6d) at 0400 July 19, and there existed a 350-hPa upright positive vorticity column in correspondence to the precipitation centre (Fig. 6a). This vorticity band was intense with its principal part over the sea. With the movement of the typhoon, this vorticity band gradually moved to the continent, which in turn amplified the precipitation in the southern centre of the rainfall. At 0700 July 19 (figure omitted), there existed an inflowing radial wind with the greatest intensity of –25m/s, which was under 700 hPa and 250 to 450 km away from the centre. Due to the effect of strong radial wind, the upright positive vorticity column gradually moved inward, with a radial speed of 15 m/s. The transient inward (outward) transmission of waves in the radial direction has been found in many studies[10-11]. This is related to the topography, the advection effect of radial wind, the strengthening of moist baroclinity and the releasing of the latent heat from the ascending warm and wet airstream. What corresponds with the inward transmission of the positive vorticity column is the fact that the precipitation on the inner rim of outer spiral rain bands strengthens gradually as well (figure omitted).

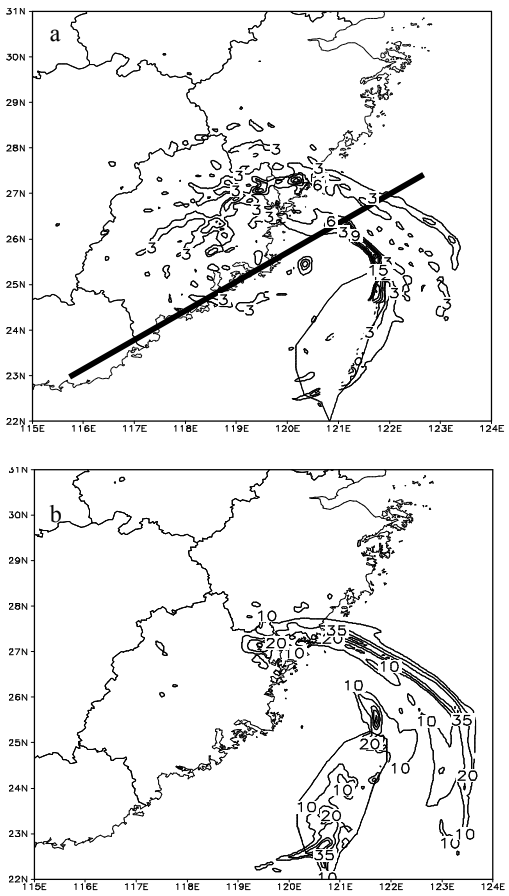

Fig.5 850-hPa positive vorticity (unit: 10^{-4} s^{-1}) and rainfall for one hour simulated by fine grids (unit: mm, intervals: 10 mm) Notes: Black triangle: centre of typhoon; black line: location of the radial cross section passing the centre. a: vorticity at 0400 July 19; b: precipitation amount from 0300 to 0400 July 19.

At the lower level, the radial wind with the central value of −30 m/s existed outside of the primary vorticity column at 1000 July 19 (Fig. 6b). However, this positive vorticity column did not transmit inward under the effect of radial wind, but occurred 300 km away from the centre. Its intensity strengthened and the central value was up to 2.4×10^{-3} s^{-1}. Another weaker vorticity column (secondary vorticity column) was found outside below 600 hPa, which was 100 km away from the primary vorticity column (the strong vorticity column 300 km away). Two relatively obvious vorticity columns were formed radially. What corresponds with these two positive vorticity columns is the intensive precipitation in the two areas (Fig. 6e). Especially, the precipitation was up to 100 mm near the primary vorticity column and above 40 mm near the secondary vorticity column. The two precipitation bands were in correspondence with the two spiral rain bands, which in turn corresponded with the southern and northern precipitation centres on the continent.

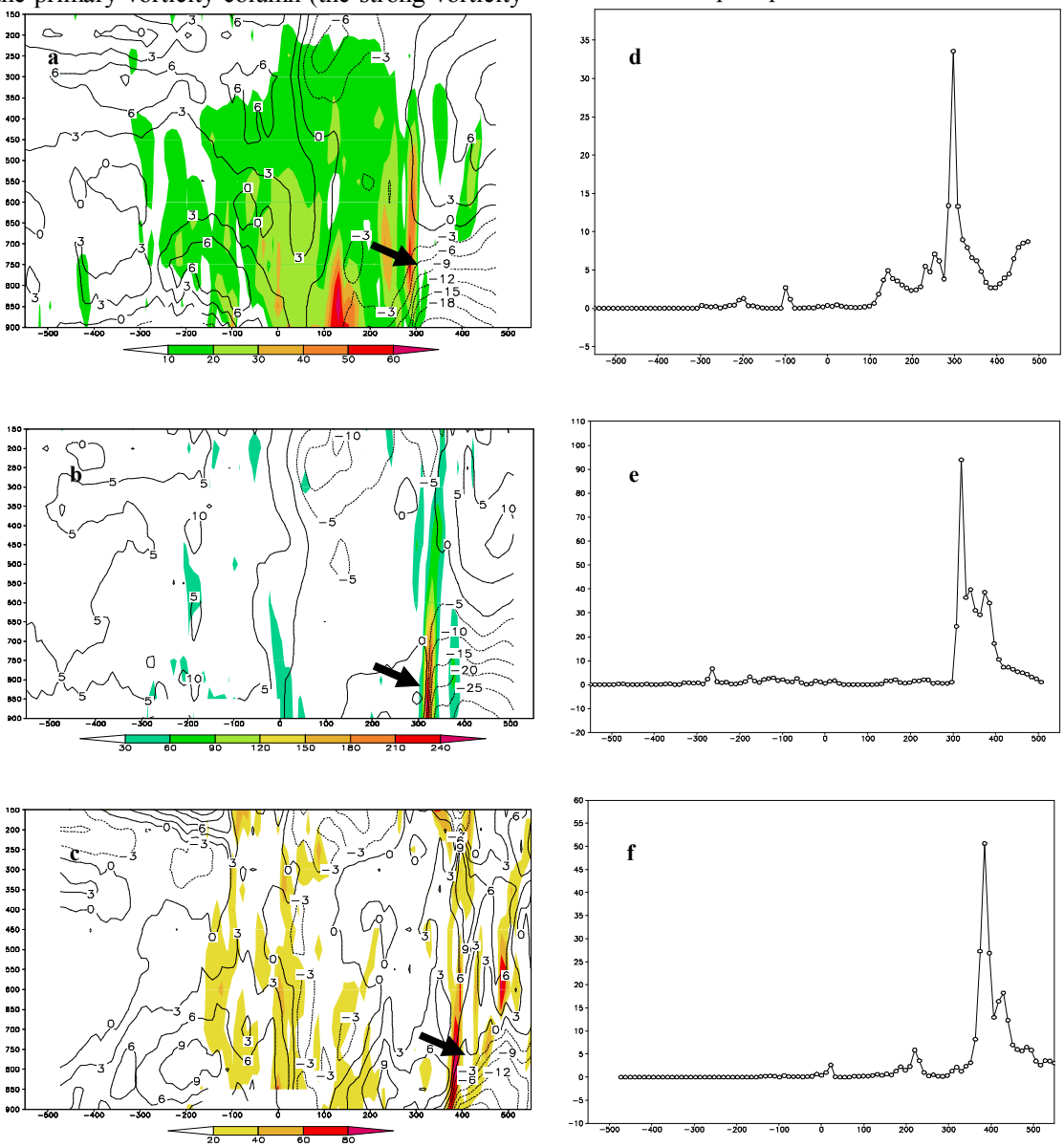

Fig.6 Positive vorticity at 0400, 1000, and 1600 July 19 (shadow areas, unit: 10^{-5} s^{-1}) and vertical distribution (a, b, c) of the radial wind (isoline, broken line: radial inward flow; solid line: radial outward flow; unit: m/s) in the radial direction. The precipitation distribution (unit: mm) at 0400, 1000, and 1600 July 19 (d, e, f).
Notes: Point 0 is the geometrical centre of the typhoon, the broad-brush arrowheads in panels (a) to (c) point to the primary vorticity columns (the maximum of vorticity) at different hours. The abscissa shows the radial distance to the centre of typhoon (unit: km) and the ordinate shows the height of the barosphere (panels (a) to (c), unit: hPa)

Possibly because the vertical shear of the wind increased and the moist baroclinity strengthened, bringing about the development of vertical vorticity[12], the primary vorticity column did not transmit inward but outward under the circumstances of intensive inflow radial wind. Within a range of 300 to 500 km around the typhoon centre below 600 hPa, because of the landing of the typhoon (at 0900 July 19), relatively

strong pressure gradients were formed between the northern side of the typhoon and the subtropical high on the continent, which in turn increased horizontal and vertical gradients of the inflow radial wind within this range (Fig. 6b). 300 to 450 km from the centre, the gradient equivalent potential temperature line (Fig. 7a) slanting in the lower part of the troposphere appeared, together with greater vertical gradients of the radial wind. This fact shows that the slanting vertical vorticity triggered by the changes of moist baroclinity developed here. The dense equivalent potential temperature contours descended towards the lower levels, forming the shape of a funnel (Fig. 7a), which showed that 320 km near the centre, because of the saturation of the vapour in the deep wet convection, the strong precipitation released great deal of latent heat, causing the downward extension of the warm tongue in the higher levels. What corresponds with the ascending movement of the strong convection above the two positive vorticity columns are two positive divergence columns slanting outward along with the height increasing from the middle to higher levels (Fig. 7b). With a central value of 250 hPa, the divergence columns are up to $6.0\times10^{-4}s^{-1}$ in height, and the relatively intense divergence serves to 'ventilate', which contributes to low-level convergence and intense precipitation.

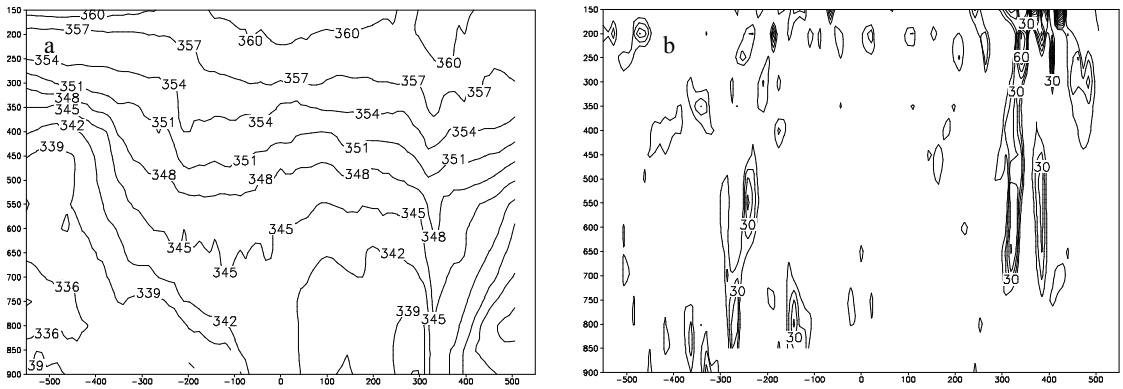

Fig.7 The potential temperature passing the centre of typhoon (a, unit: K); the value of divergence (b, unit: 10^{-5} s^{-1}) radial vertical cross section.

It is known from 1300 (figure omitted) to 1600 (Fig. 6c) July 19, inside the primary vorticity column, the outflow radial wind gradually strengthened. Under the impact of radial flows in the opposite direction, the two vorticity columns gradually combined. The TBB figure (Fig. 2c) showing what actually happened indicated that the rain bands combined after the landing of the typhoon. At 1300 July 19 (figure omitted), two vorticity columns combined at the height of 900 hPa, but their distance grew with the increase of height. The combination of these two vorticity columns corresponded to the combination of the rain bands (figure omitted), causing greater precipitation at the point of the combination. The precipitation was up to 90 mm per hour 420 km from the centre. From Fig. 6c it could be found that at 1600 July 19, 400 km from the centre and outside of the strong vorticity column, because the inflow radial wind strengthened, two nearby vorticity columns combined below 800 hPa but separated again above this height. Figure 6f showed that a weaker precipitation centre occurred 430 km from the centre; the vorticity columns combined in the low levels and separated in the high levels, and their combination brought about more precipitation, with weaker precipitation areas also occurring. The reason for the aforementioned fact could be that above where the combination happened, the upward movement strengthened and thus the latent heat was released, which led to the fact that the diabatic heating caused a greater distance between spiral rain bands and therefore pushed them to a broader area. This conclusion was verified in the numerical experiment by Diercks and Anthes.[11].

Figure 6c indicates greater horizontal gradient of the radial wind below 700 hPa 400 to 500 km from the centre. According to the imbalance theory of gradient wind, super-gradient flows and radial inflowing air will move upward in the convergence area. Under the effect of Earth's rotation, above the area of dense radial wind gradients, an area of dense tangential wind gradients could be generated. At 1600 July 19, an area of dense tangential wind gradients was located between 800 hPa and 550 hPa, with a maximum value of 30 m/s (Fig. 8).

Figure 6 shows that there was an ideal correspondent relationship between rain bands and positive vorticity bands at the lower level, while the precipitation was only distributed asymmtrically on one side of the typhoon. This might be attributed to the constraints of dynamics, thermodynamics and water vapour.

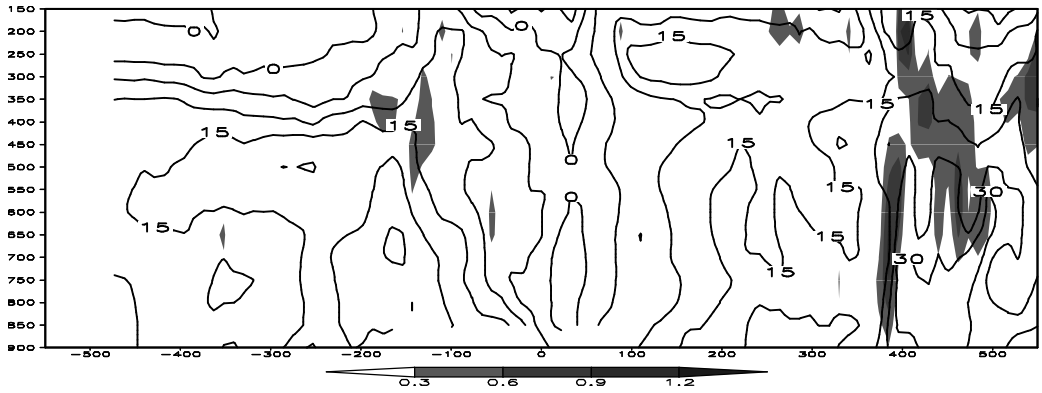

Fig.8 Vertical rising speed passing the centre of typhoon (shadow area, unit: m/s); shear wind (isoline, unit: m/s).

3.2 *Relationship between the distribution characteristics of the wind field and asymmetric rain bands*

In Wu et al. [13], the author holds that there exists correspondence between asymmetric structure and the slanting of eddy's direction caused by the shear. According to Ding et al.[14], the asymmetric structure in the outskirt is mainly caused by the pressure field configuration of large scale synoptic systems in the environment field. In order to observe the relationship between rain area distribution and wind field of the typhoon at higher and lower levels under the impact of peripheral systems, a figure illustrating the vertical shear wind field between 200 hPa and 850 hPa, the divergence field of the vertical shear and the distribution of precipitation areas, is drawn.

If $\overrightarrow{V'} = u'\vec{i} + v'\vec{j}$, $u'\vec{i} = u_{200hPa}\vec{i} - u_{850hPa}\vec{i}$, $v'\vec{j} = v_{200hPa}\vec{j} - v_{850hPa}\vec{j}$, then

$$\nabla \cdot \overrightarrow{V'} = \frac{\partial}{\partial x}(u_{200hPa} - u_{850hPa}) + \frac{\partial}{\partial y}(v_{200hPa} - v_{850hPa}), \text{ i.e. } \nabla \cdot \overrightarrow{V'} = \nabla \cdot \vec{V}_{200hPa} - \nabla \cdot \vec{V}_{850hPa}.$$

The divergence field of the vertical shear is the algebraic difference between divergence fields at 200 hPa and 850 hPa, respectively. If $\nabla \cdot \overrightarrow{V'} > 0$, it shows that at higher levels the wind field diverges in relation to the lower-level wind field, and the ventilation effect which depressurizes higher-level dynamics favours the upward movement of the convergence at low levels. The stronger the vertical shear is, the greater its divergence at high levels is. Figure 9 showed that the strongest area of precipitation corresponded to the divergence centre of the vertical shear. At 1300 July 19 the maritime central value of the divergence is up to 1.2 $\times 10^{-3}s^{-1}$, the precipitation amount was over 100 mm per hour (Fig. 9b). It can be seen from the figure that the divergence centre was mainly located at the northern (north-east) side of the circulation of the typhoon, and rather unobvious at the southern side. Therefore its divergence field was asymmetric. Although there were many scattered divergence centres at the north-west side of the typhoon circulation, for the lack of vapor, the precipitation amount was not big. When there were enough vapor and continuous spiral divergence bands at the north-east side, the precipitation was intense. Here the warm and wet air current ascends and coagulates, together with the releasing of latent heat, making high-level divergence stronger and $\nabla \cdot \overrightarrow{V'}$ bigger. There is a positive feedback mechanism between high-level divergence and the releasing of latent heat caused by the coagulation of ascending warm and wet air currents. This makes the asymmetric distribution of precipitation in the north and south even obvious.

Figure 12a showed that in the southern precipitation centre, the precipitation reached its maximum at 0600 to 0700 July 19, i.e. over 40 mm per hour. Figure 10a indicates that at this centre, the convergence layer is below 800 hPa and the central convergence value is $-3.0\times10^{-4}s^{-1}$ at 850 hPa. The divergence layer is from 700 hPa to 300 hPa, with a central value of $5.0\times10^{-4}s^{-1}$ in the middle layer of the troposphere. It changed into a convergence layer above 200 hPa. This divergence configuration favors intensive precipitation. The north-east wind was mainly at the lower levels while there was east wind in the middle level and low-speed south-east wind at higher levels. The obvious clockwise shear between the lower and higher levels favoured the dynamic environment for the convection at the east side of the typhoon. The convergence field at higher levels extended downward at 1300 to 1700, and descended to 550 hPa at 1500 (Fig. 10a). This movement conveyed the momentum downward, causing the wind speed within the

convection to become uniform. The vertical clockwise shear decreased and $\nabla \cdot \overline{V}'$ also became smaller. The convergence and descending field at the high level extended downwards and therefore restrained the upward movement of convection at the low level. This explains the obvious subsiding of precipitation during this period of time (as shown in Fig. 12a). Figure 12b showed that in the northern precipitation centre the precipitation became stronger from 0600, over 30 mm between 1100 and 1200. From 0600 to 0900 the convergence layer extended upward, and at 0700 the convergence centre was located around 650 hPa. After 0900, the height of convergence centre gradually descended with time, and between 1000 and 1600 it was below 850 hPa (Fig. 10b). The descending of the convergence layer and the strengthening of its intensity corresponded to the intensive precipitation at this time (Fig. 12b).

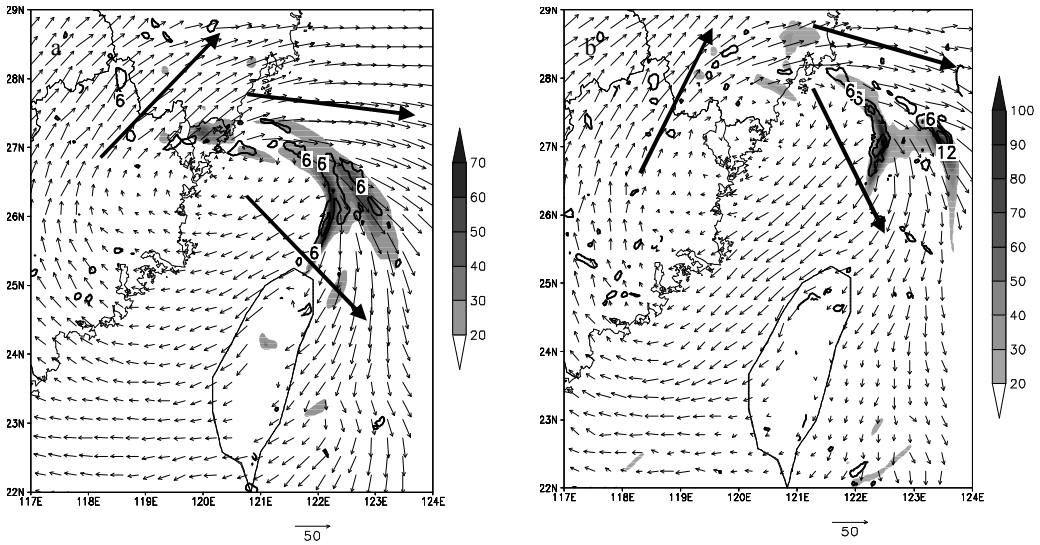

Fig.9 Vertical $\overline{V}_{200hPa} - \overline{V}_{850hPa}$ wind shear field (vector graph), precipitation distribution (shadow area, unit: mm) and divergence field of the vertical wind shear (isoline, unit: 10^{-4} s^{-1}) at 0700 (a) and 1300 (b).

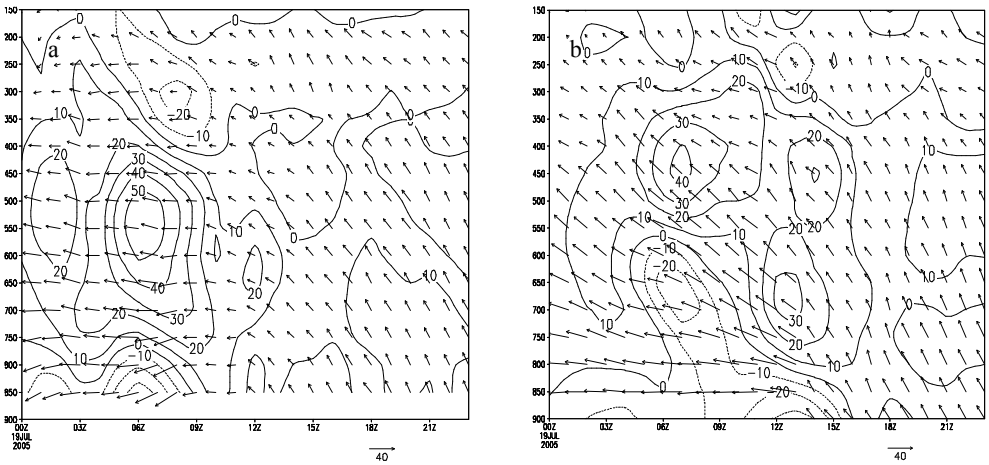

Fig. 10 Vertical cross sections of the horizontal wind field (vector graph) and divergence field (isoline, unit:10^{-5} s^{-1}) in the southern precipitation centre (a) and the northern precipitation centre (b).
Notes: abscissa: time; ordinate: barosphere (unit: hPa)

Many researches [15-17] have taken into account the relationship between the moving path of typhoon and the asymmetric precipitation. From 0000 July 19 to 0000 July 20, Haitang basically moved north-westward and its asymmetric wind speed band was mainly located to the north-east of the centre (figure omitted). A strong wind speed band with a central value of 40 m/s passed the southern precipitation centre at 07:00 (figure omitted). The horizontal shear caused by the strong wind speed band corresponded with the intensive positive vorticity bands and rain bands at the low level. The spiral high wind with a central value of 30 m/s passed the northern precipitation centre (121°E, 28.2°N) at 1500 (figure omitted), corresponding to the precipitation increase. The easterly jet stream band at the low level brought abundant water vapour from the ocean, together with the divergence field of the asymmetric vertical wind shear wind, making the rain

bands asymmetric.

4 DIAGNOSTIC ANALYSIS OF CVV OF THE RAINSTORM CENTRE

Because the precipitation in the simulated southern precipitation centre on the continent is strong, the positive vorticity band at 850 hPa is called the primary vorticity band, which corresponds to the primary vorticity column 300 km away from the centre of the typhoon in Fig. 6b. The 850-hPa positive vorticity band where the northern precipitation centre is located is called the secondary vorticity band, which corresponds to the secondary vorticity column in Fig. 6b. In Zhao and Gao[8], CVV was used to track the development and evolvement of a large-scale rainstorm system in North China Plain. It was found that the vertical component of CVV has a rather close relationship with the area of the rainstorm. The vertical component of CVV could be expressed on the coordinate Z as

$$C_z = \frac{1}{\rho}[(\frac{\partial w}{\partial y} - \frac{\partial v}{\partial z})\frac{\partial \theta_e}{\partial y} - (\frac{\partial u}{\partial z} - \frac{\partial w}{\partial x})\frac{\partial \theta_e}{\partial x}],$$

and $\frac{\partial w}{\partial y}$ and $\frac{\partial w}{\partial x}$ could be omitted because of their small values. To match the output data type of the model, the vertical component of CVV is converted into the equation on the coordinate P as

$$C = g[\frac{\partial v}{\partial p}(\frac{\partial \theta_e}{\partial y} + \frac{p}{RT_v}\frac{\partial \theta_e}{\partial p}\frac{\partial \phi}{\partial y}) + \frac{\partial u}{\partial p}(\frac{\partial \theta_e}{\partial x} + \frac{p}{RT_v}\frac{\partial \theta_e}{\partial p}\frac{\partial \phi}{\partial x})],$$

and ϕ refers to the potential height and T_v refers to the virtual temperature in correspondence with saturated moist air.

Figure 6 showed that at different hours in the precipitation areas, the vertical shear of the 750-hPa radial wind in the lower troposphere was relatively intense and Fig. 7a showed that the strong rainstorm twisted the equivalent potential temperature contour abruptly in the low- and mid-troposphere and increased the horizontal gradients of equivalent potential temperature. The horizontal gradient of the wind speed at 750 hPa was also large in the precipitation centres (figure omitted). Based on the above factors, the vertical component of CVV at 750 hPa was used to track the temporal variation of precipitation in the southern and northern precipitation centres.

From Fig. 12a it could be seen that the precipitation in the southern precipitation centre reached its maximum at 0700 July 19, mainly because the intensive maritime positive vorticity band at 850 hPa combined with the continental precipitation band where the southern precipitation centre at 0600 July 19 (Fig. 2b). The precipitation in the southern precipitation centre was intensive from 0200 to 1000 July 19 and gradually weakened as the rain band moved toward the north. Figure 12b showed that the precipitation in the northern precipitation centre acquired its maximum at 1500 to 1600 July 19, mainly because the primary southern rain band gradually moved north and combined with the northern secondary rain band at 1500 to 1600 July 19 (Fig. 6c), showing that the movement of the rain bands directly affected the amplification of the precipitation. From Fig. 12b we could also see that south of the northern precipitation centre (near the latitude of the southern precipitation centre), there was also intensive precipitation before 0900 July 19, indicating that there had been many rain bands before the landing of the typhoon, in correspondence with the distribution of several cloud bands observed (Fig. 2a).

By comparing Fig. 11 with Fig. 12, we found that the amount of precipitation near the southern and northern precipitation centres reached its maximum 1 or 2 hours earlier than the vertical component of CVV amounted to its maximum. The vertical component of CVV represents the dynamics and thermodynamics of the rainstorm and the amount of precipitation corresponds with a dense area of the gradient of the vertical component of CVV. With abundant water vapour (figure omitted), the rising saturated moist air increased $\frac{\partial \theta_e}{\partial y}$. The order of magnitudes of $\frac{\partial \theta_e}{\partial y}$ (figure omitted) is similar to that of the vertical component of CVV, so are their trends of change, but the former arrives at its maximum earlier than the latter. This corresponds with the fact that the precipitation comes to its peak value earlier than the vertical component of CVV.

During this typhoon rainstorm, there existed certain spatial and temporal discrepancies between the evolvement of the vertical component of CVV and that of the precipitation process, but they are basically consistent. Therefore, they could be used to have a good track of the transformation trend of the precipitation

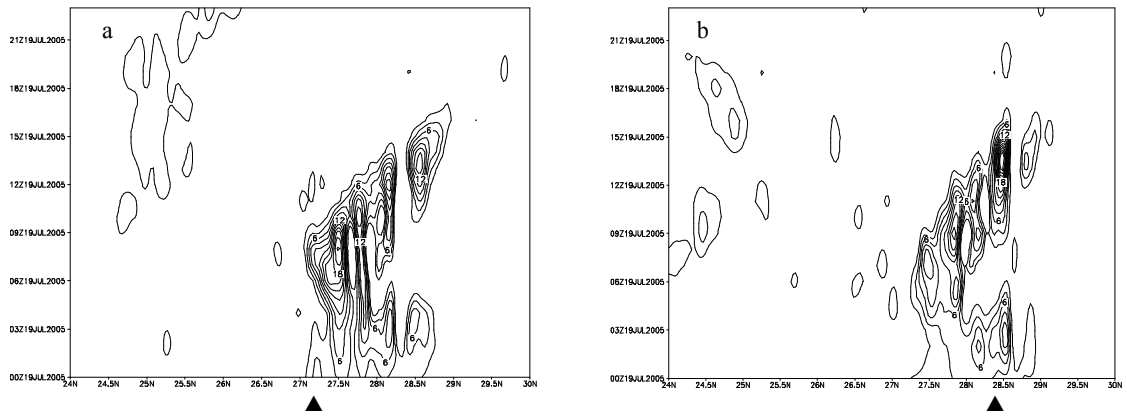

Fig.11 Longitudinal cross section of 120°E (a) for 750-hPa vertical component of CVV (positive value distribution, unit: $10^{-3}\cdot m\times s^{-3}\cdot K\cdot hPa^{-1}$) varying with time (a) and of 121°E (b).
Notes: left black triangle: southern precipitation centre; right black triangle: northern precipitation centre.

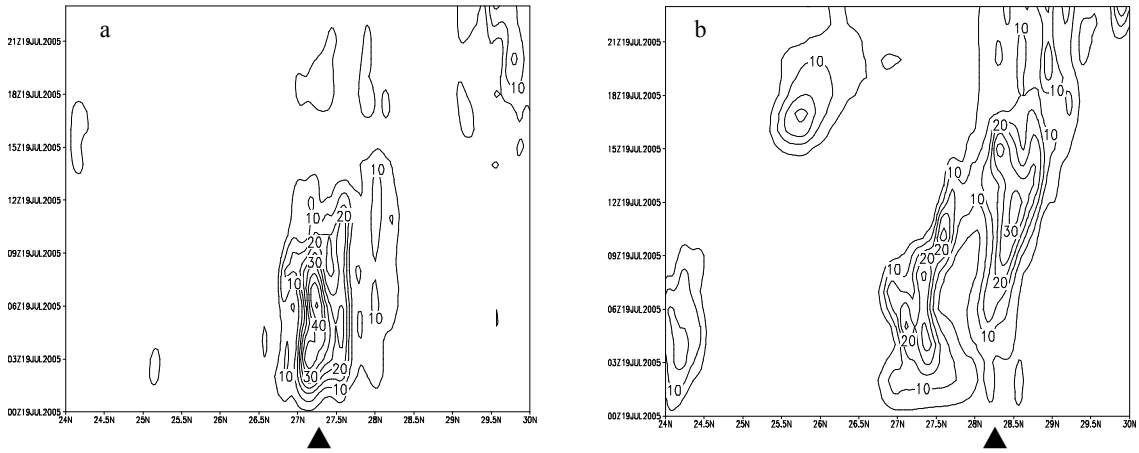

Fig.12 Longitudinal cross sections of precipitation (unit: mm) at 120°E which varies with time (a); longitudinal cross sections of precipitation rain fall (unit: mm) at 121°E varying with time (b).
Notes: left black triangle: southern precipitation centre; right black triangle: northern precipitation centre.

The change of the precipitation and the moving trend of rain bands in the northern precipitation centre (Fig. 12b) had a better correspondence with the vertical component of CVV (Fig. 11b) than those in the southern one. The precipitation affecting the northern precipitation centre mainly occurred after the landing of the typhoon. After this point, the horizontal temperature gradient grew bigger because of the encounter between the typhoon and cold air from the north; the vertical shear of wind speed between the typhoon and the northern high system became stronger; the moist baroclinity of the longitudinal vertical circulation at the northern side of the typhoon turned even more obvious. Because the vertical component of CVV represents the changing features of the systemic secondary circulation and horizontal moist baroclinity, the above conclusion is drawn.

5 CONCLUSIONS

There exists a direct relationship between the typhoon precipitation and the structural characteristics of the bi-(multi-) spiral rain bands in the periphery of typhoon. Through an analysis of this case, the following conclusions can be reached:

(1) The periphery rain bands, especially the primary rain bands in the south, moved in correspondence with the 850-hPa positive vorticity band (the upright positive vorticity column at the low level). The movement of the spiral rain bands in the radial direction was related with the intensity of the radial wind, the strengthening of the moist baroclinity and the fact that the saturated vapour coagulated into precipitation and released latent heat. The combination of the rain bands brought about the amplification of the precipitation on the continent.

(2) The asymmetric structure of the spiral rain bands was related with the asymmetric distribution of the horizontal wind speed gradient and channels of water vapor. Besides, the divergence field of the

vertical wind shear had a "ventilating" effect, which favoured the upward movement of the convergence at the low level.

(3) The vertical component of CVV at the low level (750 hPa) where strong wind bands were located could well be used to track the precipitation and the position of the rain bands in the rainstorm areas because the dense horizontal gradients of equivalent potential temperature and comparatively intense vertical wind shear contributed to the vertical component of CVV.

Acknowledgement: The authors would like to express our heart-felt gratitude to Ms Wu Wenjun (School of Language and Culture, NUIST) for her painstaking effort in rending this thesis from Chinese into English. Her excellent skill in Chinese-English translation has guaranteed the linguistic quality of this thesis in its English version. Our thanks also goes to Prof Fan Yong (School of Language and Culture, NUIST) for doing an arduous job in revising and finalizing the English version.

REFERENCES:

[1] LI Ying, WANG Ji-zhi, CHEN Lian-shou, etal. Characteristic analysis of the undulant precipitation of typhoon "Matsa" [J]. Sci. Bull., 2007, 52(3): 344-353.
[2] ZHU Pei-jun, ZHENG Yong-guang, WANG Hong-qing et al. Numerical simulation of typhoon spiral rain bands [J]. Sci. Bull., 2005, 50(5): 486-494.
[3] ZHU Pei-jun, CHEN Min, TAO Zu-yu, et al. Numerical simulation of typhoon "Winner" (1997) after landfall PartⅡ: structural evolution analysis [J]. Acta Meteor. Sinica, 2002, 60(5): 560-567.
[4] YU Zhi-ao. The spiral rain band of tropical cyclone and vortex Rossby waves [J]. Acta Meteor. Sinica, 2002, 60(4): 502-507.
[5] DENG Lian-tang, LIU Shi-shi, XU Xiang-de, et al. The role of Rossby parameter in vortex Rossby waves [J]. J. Trop. Meteor., 2004, 20(5): 483-492.
[6] KANG Jian-wei, LU Han-cheng, ZHONG Ke, et al. The meso-scale waves and the formation of polygonal eye wall in typhoon [J]. J. Trop. Meteor.(in Chinese), 2007, 23(1): 21-26.
[7] SUN Shu-qing, ZHOU Yu-shu. Advances in Meso-Scale dynamical analysis of torrential rain systems in recent years in China [J]. Chin. J. Atmos. Sciences, 2007, 31(6): 1171-1188.
[8] ZHAO Yu, GAO Shou-ting. Application of the convective vorticity vector to the analysis of a rainstorm [J]. Chin. J. Atmos. Sci., 2008, 32(3): 444-456.
[9] WANG Yong, DING Zhi-ying. Structural and characteristic analyses of spiral rain bands around the landing of typhoon "Haitang" [J]. J. Nanjing Inst. Meteor., 2008, 31(3): 352-362.
[10] YU Jin-hua, TAN Zhe-min. Island-like topographic effects on the propagation of vortex Rossby waves [J]. J. Nanjing Uni. (Nat. Sci.), 2007, 43(6): 597-605.
[11] DIERCKS J W, ANTHES R A. A Study of Spiral Bands in a Linear MODEL OF A Cyclonic Vortex [J]. J. Atmos. Sci., 1976, 33(9): 1714-1729.
[12] WU Guo-xiong, CAI Ya-ping, TANG Xiao-jing. Moist potential vorticity and slantwise vorticity development [J]. Acta Meteor. Sinica, 1995, 53(4): 387-405.
[13] WU Li-guang, BRAUN S A, HALVERSON J, et al. A Numerical Study of Hurricane "Erin" (2001). Part: Model Verification and Storm Evolution [J]. J. Atmos. Sci., 2006, 63(1): 65-86.
[14] DING Jin-cai, YAO Zu-qing, TANG Xin-zhang. The analysis of the asymmetric structure of tropical cyclone "DOUG" and its influence on precipitation [J]. Acta Meteor. Sinica, 1997, 55(3): 379-384.
[15] ZHANG Sheng-jun, CHEN Lian-shou, XU Xiang-de. The Diagnostic Analysis and Numerical Simulation of the Unusual Track of "HELEN" (9505) [J]. Chin. J. Atmos. Sci., 2005, 2 9(6): 937-946.
[16] CORBOSIERO K L, MOLINARI J. The Relationship between Storm Motion, Vertical Wind Shear, and Converctive Asymmetries in Tropical Cyclones [J]. J. Atmos. Sci., 2003, 60(2): 366-376.
[17] YU Zheng-shou, CHEN Min, YE Zi-xiang, et al. Analysis of rainstorm associated with tropical cyclones "HAITANG"(0505) and "BILIS"(0604) which were of similar paths [J]. J. Trop. Meteor., 2009, 25(1): 37-47.

Citation: WANG Yong, DING Zhi-ying, LI Xun et al. Diagnostic analysis of asymmetric spiral rainbands around the landing of typhoon Haitang (2005). *J. Trop. Meteor.*, 2010, 16(2): 143-153.